

Nonlinear kinetic simulation study of the ion-ion streaming instability in single- and multi-ion species plasmas

T. Chapman, R. L. Berger, A. Dimits, I. Joseph, and D. Ghosh

Lawrence Livermore National Laboratory, P.O. Box 808, Livermore, CA 94551, USA^{a)}

B. J. Winjum

Institute for Digital Research and Education, University of California Los Angeles, Los Angeles, California 90095, USA

J. W. Banks

Department of Mathematical Sciences, Rensselaer Polytechnic Institute, 301 Amos Eaton Hall, Troy, NY 12180, USA

S. Brunner

Swiss Plasma Centre, École Polytechnique Fédérale de Lausanne, Station 13, CH-1015 Lausanne, Switzerland

(Dated: 9 September 2020)

The nonlinear evolution of the ion-ion streaming instability (IISI) is studied using numerical techniques novel to this problem that afford direct insight into the evolution of the particle distributions of each species. During the linear phase of the instability, we demonstrate quantitative agreement with linear kinetic theory. Subsequently, the electrostatic field generated by the IISI causes ring-like velocity distributions of ions to form that are both heated and slowed to varying degrees relative to their initial flows. Due to variation in the trapping conditions for ion species of differing charge-to-mass ratio, when flows of multiple species interact, the nonlinear evolution of each species can be starkly different: we show a case where a lighter ion species is completely stopped by a heavier ion species via the IISI alone (i.e., without collisions) and, for the first time, demonstrate how the IISI can introduce a relative flow between ion species that initially have same flow velocities, thereby separating them.

I. INTRODUCTION

The electrostatic instability driven in plasma by ions that counterstream at approximately sonic speeds is of interest in several active research areas due to its ability to excite a large electrostatic potential and heat ions. Laboratory experiments^{1–3} using opposed laser-irradiated foils have demonstrated the efficacy of the ion-ion streaming instability^{4,5} (IISI) to increase ion temperatures at rates that can not be explained by collisional (fluid-like) processes in the counterstreaming plasma. Collisionless shocks, where ions are reflected and counterstream at the shock interface, are thought to be present in many astrophysical contexts with scales ranging from the Earth's bow shock to galactic clusters, and have long been investigated as an explanation for observed cosmic ray spectra^{6–10}. Similarly, collisionless shocks have recently been utilized in proof-of-principle experiments^{11–13} to generate high-quality ≥ 10 MeV proton beams. The IISI can lead to the breakup of such shocks^{14,15} and has been suggested as a mechanism of enhanced ion acceleration¹⁶.

The IISI can be saturated by both ion heating^{4,5,17–19} and ion trapping^{5,20}. The two mechanisms are not independent: ion trapping can convert the electrostatic energy of the ion waves into particle kinetic energy (which, after phase space filamentation and subsequent diffusion

in velocity, can be viewed as a change in temperature that is generally anisotropic), while a change in ion temperature will alter the magnitude of all wave-particle interaction processes in addition to directly stabilizing the IISI.

In the following, we demonstrate various nonlinear behaviors of the IISI, covering saturation, sensitivity to initial flow velocity, and the unique consequence of ion trapping when ion species of different charge-to-mass ratios are present. Our results are obtained using a fully kinetic continuum method^{21–23} that is 6th-order accurate in all phase space directions and time to describe the evolution of distribution functions. This approach is novel in the study of this instability and enables accurate diagnosis of growth rates and instability thresholds. In our simulations, we measure growth rates that agree with linear theory and show phase space structures that can be understood using simple analytic estimates of the ion trapping regions in phase space. These structures persist long after the ions are detrapped. We also show that ion trapping in a multi-ion species plasma can preferentially heat the heavier ion species and is able to dramatically alter the streaming velocity of the lighter species, offering a new species velocity separation mechanism.

We study interpenetrating streams of hydrogen (H) and carbon (C). Pure hydrogen plasmas (H-H interpenetration) are commonly occurring in a variety of applications, so make a natural case of interest. To exhibit the phenomena that arise when ions of differing mass (and, importantly, charge-to-mass ratio) are present, we

^{a)}email: chapman29@llnl.gov

case	mats.	u/c_s	$k_{ }^{max} \lambda_{De}$	$k_{\perp}^{max} \lambda_{De}$	$\gamma_k^{max}/\omega_{pi}$	$\omega_k^{max}/\omega_{pi}$
1	H/H	0.51	1.08	0	0.14	0
2	H/H	0.88	0.68	0.68	0.16	0
3	H/H	2.57	0.23	0.93	0.16	0
4	C/H	0.64	0.68	0.82	0.11	0.031
5	CH ₂ /CH ₂	0.64	0.57	1.24	0.13	0

TABLE I. Plasma properties and calculated linear kinetic ion-streaming instability quantities for the cases addressed in this paper, where ions stream at velocities $\pm u$. For each case, $T_e/T_i = 20$ at the beginning of the simulation. The reference quantities $c_s = \sqrt{T_e/m_p}$ and $\omega_{pi} = \sqrt{4\pi n_e e^2/m_p}$ are the same for all cases.

study interpenetration where one stream is pure H and the other pure C. To demonstrate velocity separation via the IISI, we also present results from two interpenetrating streams of CH₂; this material is also common in experiments featuring laser-driven plasma expansion, such as in Refs. 1 and 2. While here we limit our study to neutral fully ionized plasmas, the numerical methods and analysis employed is of relevance to streaming instabilities in negative-ion plasmas²⁴ (electrons, positive ions, and negative ions) and pair-ion plasmas^{25,26} (positive and negative ions only).

The layout of this article is as follows: First, the plasma parameters of focus here are introduced. Linear quantities, such as growth rates and the wave vector at which the maximum growth rate occurs, are calculated. The simulation method is then discussed. Next, results from hydrogen streams of differing initial flow velocity are presented, followed by hydrogen-carbon mixtures. Finally, we summarize and discuss the implications of our results.

II. PLASMA PARAMETERS AND SIMULATION METHOD

We study the IISI using i) two counterstreaming flows of hydrogen with a range of initial relative flow speeds u that change the qualitative behavior of the IISI, and ii) counterstreaming flows of hydrogen and carbon. To remove ambiguity, electromagnetic (Weibel) instabilities are precluded by choosing to solve a Vlasov-Poisson system. The Weibel instability is typically slow compared to the IISI²⁷, meaning that the IISI will generally saturate before the subsequent onset of the Weibel instability¹⁴.

Due to the timescales considered as well as for simplicity, the plasma is treated as collisionless. The system is discretized in two Cartesian space and velocity dimensions (2D2V) and solved using the LOKI^{21–23} code. Continuum methods are not subject to numerical noise above machine precision and our simulations are therefore free of spurious heating, although we introduce thermal fluctuations to provide a broad-spectrum initial density perturbation [these density perturbations are $\mathcal{O}(10^{-8})$ in

Fourier space]. The 6th-order scheme permits larger grid point intervals in space and time for a given numerical accuracy than lower-order methods. The latter property is particularly desirable due to the computationally demanding fully kinetic description of both the electrons and the ions (with a physical mass ratio) in our simulations. Simpler quasilinear descriptions lack the necessary physics of ion trapping⁵. In addition to the 2D2V Vlasov simulations presented here, we were also able to reproduce the nonlinear states using the particle-in-cell code OSIRIS²⁸.

The plasma is initially homogeneous apart from the initial low density fluctuation level. The spatial boundaries are chosen to be periodic, permitting an unambiguous view of the instability, similar to Ref. 29. The velocity grids are truncated at a maximum and minimum velocities for each species (see Table II) that are of sufficient magnitude such that the details of the boundaries are unimportant to the solution; details are provided in Ref. 23. In all cases, the distribution functions of the electrons and ions must be evolved on separate grids since they have different masses and charges. For H/H interpenetration (but not C/H or CH₂/CH₂), one may choose to evolve the two ions streams as a single combined distribution function or as two separate distribution functions; we confirmed that this choice has no bearing on the solution, although for diagnostic purposes, evolving the two ion streams separately is convenient and instructive.

The plasma properties are summarized in Table I. In all cases, the plasma is fully ionized. The plasma is initialized in a frame where there are two (or four, as in case 5) shifted isotropic Maxwellian ion distributions of number density n_i and temperature T_i , counterstreaming with velocities $\mathbf{u}_i = (\pm u, 0)$. For all cases, n_i is equal in each flow. The electrons are initialized with a single charge-neutralizing and current-canceling Maxwellian distribution of temperature T_e , and are hot relative to

case	$\tilde{L}_{ }$	\tilde{L}_{\perp}	$\tilde{v}_{H, }^{b\pm}$	$\tilde{v}_{H,\perp}^{b\pm}$	$N_{v_{H,d}}$	$\tilde{v}_{C, }^{b\pm}$	$\tilde{v}_{C,\perp}^{b\pm}$	$N_{v_{C,d}}$
1	29.2	62.8	± 2.1	± 1.7	64	N/A	N/A	N/A
2	46.2	46.2	± 2.5	± 2.1	72	N/A	N/A	N/A
3	137	33.1	± 4.3	± 3.9	128	N/A	N/A	N/A
4	31.4	31.4	(2.1, -1.7)	± 1.7	64	(1.0, -1.2)	± 1.0	96
5	55.1	25.3	± 2.1	± 1.7	64	± 1.2	± 1.0	96

TABLE II. Numerical grid parameters. The number of spatial grid points along a given direction $d = ||, \perp$ is N_d . The number of velocity grid points of species j along direction d is $N_{v_{j,d}}$. The spatial system length along direction d is L_d . The maximum ($b+$) and minimum ($b-$) velocity grid boundaries of species j along direction d are situated at $v_{j,d}^{b\pm}$. In all cases, $N_{||} = N_{\perp} = 100$ and $N_{v_{j,||}} = N_{v_{j,\perp}}$. For the electrons, $N_{v_{e,d}} = 64$, and $v_{e,||}^{b\pm} = v_{e,\perp}^{b\pm} = \pm 6.5 v_{te}$. Ion parameters are listed in the table, where a tilde denotes normalization to λ_{De} or c_s as appropriate. The time step Δt satisfies a Courant-Friedrichs-Lewy condition and varies according to the adaptive explicit Runge-Kutta scheme, with typical values $\Delta t \sim 0.023/\omega_{pe}$.

the ions. Table I lists the wave numbers $\mathbf{k} = (k_{||}, k_{\perp})$ and growth rates γ_k of the fastest-growing (superscript “max”) Fourier modes excited by the IISI in each case. Components of vectors are defined as parallel ($||$) or perpendicular (\perp) to the flow direction. Throughout, velocities are explicitly normalized to the cold long-wave length hydrogen plasma sound speed $c_s = \sqrt{T_e/m_p}$, frequencies to the hydrogen plasma frequency $\omega_{pi} = \sqrt{4\pi n_e e^2/m_p}$, where n_e is the average electron density in the system, and distances to the electron Debye length λ_{De} . Note that for consistency these definitions of the reference quantities c_s and ω_{pi} remain fixed throughout, even when considering C/H interactions. “Hat” notation denotes a unit-vector, i.e., $\hat{\mathbf{k}} = \mathbf{k}/k$.

The kinetic dispersion relation of the system,

$$\epsilon = 1 + \sum_j \chi_j = 0; \quad \chi_j = -\frac{\omega_{pj}^2}{k^2 n_j} \int_{\mathbf{v}} \frac{\mathbf{k} \cdot (\partial f_j / \partial \mathbf{v})}{\mathbf{k} \cdot \mathbf{v} - \Omega_{kj}} d\mathbf{v}, \quad (1)$$

may be solved to find the unstable modes. Here, $\Omega_{kj} = \omega_k - \mathbf{k} \cdot \mathbf{u}_j + i\gamma_k$; $\omega_k, \mathbf{k}, \gamma_k \in \mathbb{R}$; $i = \sqrt{-1}$; and the species index j includes both electrons (e) and ions (i). $f_j = f_j(t, \mathbf{r}, \mathbf{v})$ and ω_{pj} are respectively the species distribution function and plasma frequency. t , \mathbf{r} , and \mathbf{v} are the time, space, and velocity variables. In all cases shown here, the susceptibilities $\chi_j = -[1/(2k^2 \lambda_{Dj}^2)] Z'[\Omega_{kj}/(\sqrt{2}k v_{tj})]$ are evaluated using the plasma dispersion function³⁰ Z' , where $\lambda_{Dj} = v_{tj}/\omega_{pj}$ is the species Debye length for which $v_{tj} = \sqrt{T_j/m_j}$, and T_j and m_j are the species temperature and mass, respectively. We take $m_H = m_p$, $m_C = 12m_p$, and $m_p = 1836m_e$. Standard fluid approximations to χ_i for the parameters used in cases 1-5 are only in qualitative agreement with exact numerical solutions, while for the electrons, one has $v_{te} \gg |\text{Re}[\Omega_{ke}/k]|$ and the susceptibility is well-approximated by their adiabatic response, $\chi_e \simeq 1/(k^2 \lambda_{De}^2)$. In the chosen (flow symmetric) frame, one has for cases 1-3 and 5 the real frequency $\omega_k = 0$ for unstable modes (growth rate $\gamma_k > 0$), as noted in Ref. 4, where the subscript k denotes a given Fourier mode with wave vector \mathbf{k} .

The numerical resolutions and system sizes are summarized in Table II. The spatial dimensions of the system in each case are tailored to describe the unstable modes in the system.

III. RESULTS

A. Single-ion species flows

The linear theory of IISI has been studied extensively previously^{4,5,17-19}. For identical ion streams with equal and opposite flows, the IISI requires $u \gtrsim 1.3v_{ti}$ for instability. As u is increased from this threshold, the fastest growing mode has $k_{\perp}^{max} = 0$ and the IISI is approximately

1D in nature. However, when above threshold, there are always unstable modes with $k_{\perp} > 0$ and therefore, after the system has become nonlinear, there will also be some amount of transverse ion heating (this is discussed later). For $|\hat{\mathbf{k}}^{max} \cdot \mathbf{u}_i| \gtrsim c_s$, one has $k_{\perp}^{max} > 0$ and the instability is necessarily 2D even in the linear stage of evolution. For sufficiently large u , the IISI is aligned nearly perpendicular to the flow and there are *no* unstable modes with

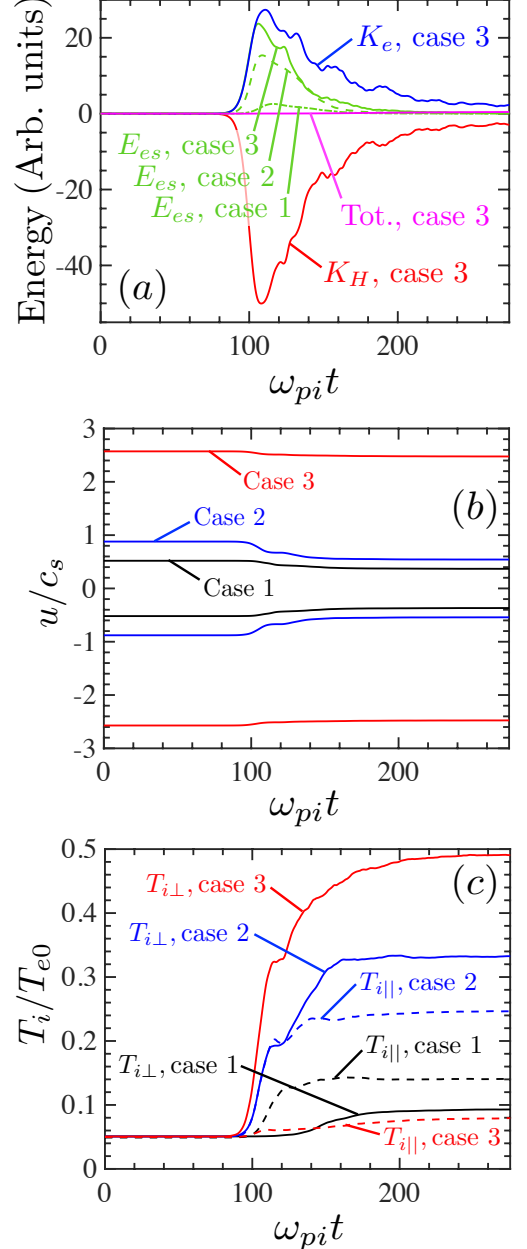


FIG. 1. (a) Changes in per-species kinetic K_j , electrostatic E_{es} , and total (Tot.) energy evolution for case 3, relative to initial values. Also shown is E_{es} for cases 1 and 2. (b) Flow velocity evolution for cases 1-3. (c) Ion heating parallel ($||$) and perpendicular (\perp) to the flow direction due to the ion streaming instability for cases 1-3.

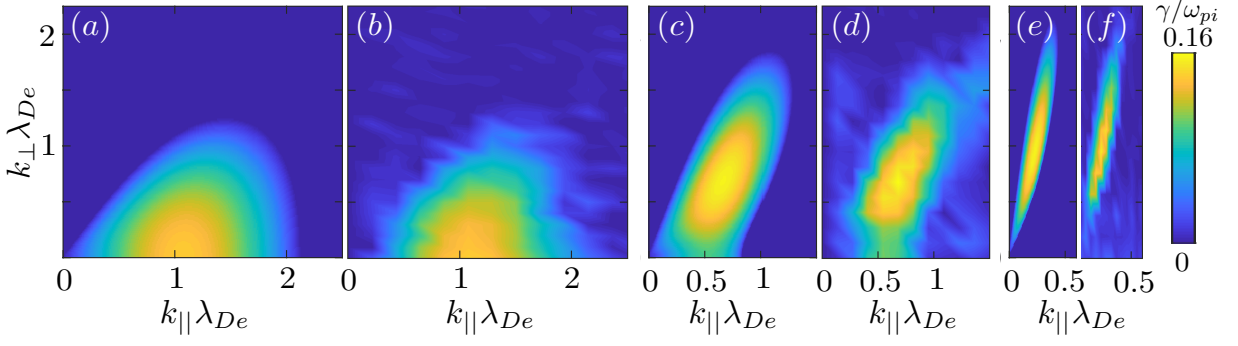


FIG. 2. For (a,b) case 1, (c,d) case 2, and (e,f) case 3, the (a,c,e) theoretical linear kinetic growth rate^{4,17} and the (b,d,f) growth rate γ of the ion streaming instability as measured in our simulations.

$k_{\perp} = 0$. In this section, we explore the nonlinear states of ion streams as u is varied between these limits. A stability criterion exists for the temperature ratio also: for $u \gtrsim 2.1v_{ti}$, instability requires $T_i/(ZT_e) \lesssim 0.28$, and this criterion becomes more stringent¹⁹ for lower u .

The evolution of the simulated system is qualitatively similar in all cases shown here: From a quiescent plasma, the IISI excites a spectrum of modes with an associated electrostatic potential. The fastest-growing modes are saturated by ions trapped in this potential (a form of “wave breaking”³¹). Since the IISI excites a spectrum of modes, a velocity phase-space diffusion then takes place with a partitioning of heating in the directions parallel and transverse to the flow that depends on \mathbf{k}^{max} (and therefore on the initial flow velocity) and the ion streams undergo some amount of slowing. The electrostatic field energy associated with the excited potential is transferred back to the particles and the IISI is fully stabilized by the increase in ion temperature. The time evolution of the electrostatic field energy, kinetic energy, flow velocity, and ion temperature are shown in Fig. 1; a detailed discussion of these quantities follows.

In Fig. 2, numerical solutions to the dispersion relation of Eq. (1) are compared with values of γ_k measured in simulations of cases 1-3 for the linear stage of growth using fits within the interval $\omega_{pi}t = [0, \sim 80]$. Measuring γ_k for the exponentially-growing unstable IISI modes in our simulations is straightforward due to the numerical method employed, where Fourier modes grow from thermal fluctuations through ~ 8 orders of magnitude before reaching saturation. An electron-ion streaming instability (EISI) is also present in the system⁴. However, the EISI is here one or more orders of magnitude slower than the IISI and does not play a role in our conclusions. Our results show no change if instead two electron populations are initialized, where each cancels the current of its associated ion stream.

The nonlinear evolution of the IISI is strongly affected by u . In Fig. 3, the hydrogen ion distributions $\langle f_i \rangle$ are shown for the three qualitatively different cases, where the ion streams are marginally subsonic (top row);

marginally supersonic (middle row); and strongly supersonic (bottom row), corresponding to cases 1-3 in Table I, respectively. $\langle \dots \rangle$ denotes averaging over all space.

The differing phase space structures can be understood by considering the electrostatic potential Φ excited by the IISI, which in turn is dictated by the most unstable wave vectors (see Table I), and the associated ion trapping. In Fig. 4a, Φ at the maximum in time of the electrostatic energy E_{es} (the time history of E_{es} is shown in Fig. 1a) is shown for case 1. In Fig. 4b, f_i sampled at $r_{\perp} = 0$ and integrated over v_{\perp} is shown, exhibiting characteristic

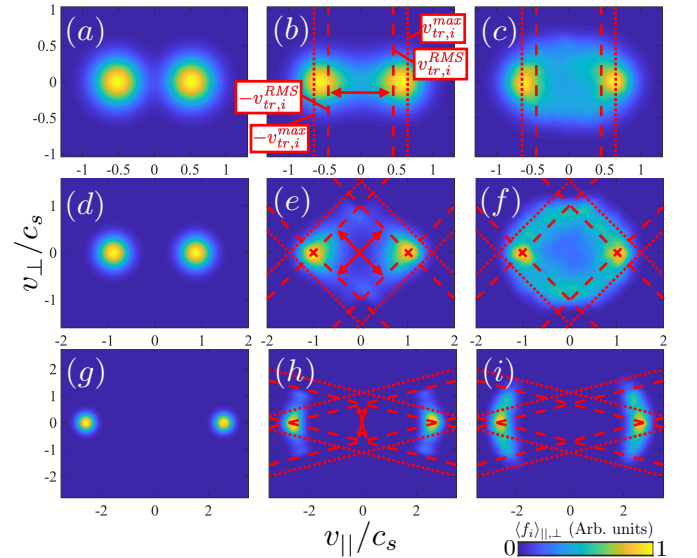


FIG. 3. Snapshots of the evolving spatially-averaged ion distribution for case 1 (top row), case 2 (middle row), and case 3 (bottom row). Shown are the initial distributions (left column), the distributions when the field energy is at a maximum (middle column), and the final state of the distribution (right column). Red lines indicate the calculated region of ion trapping associated with the maximum (max) or root-mean-squared (RMS) amplitude of the most unstable Fourier-mode in each case, while arrows indicate the direction of bounce motion.

ion trapping structures. Later in time, Φ decays to a turbulent spectrum (see Fig. 4c), the ions detrapp (see Fig. 4d), and E_{es} is converted via velocity space diffusion to particle kinetic energy, shown in Fig. 1a. In Figs. 4e and 4f, Φ at the maximum in time of E_{es} is shown for cases 2 and 3. The structures in Φ shown here correspond to large density modulations of $\sim 10\%$ in case 1 and $\sim 30\%$ in cases 2 and 3. The eventual turbulent states of cases 2 and 3 are similar to that shown for case 1.

Electrons and ions with velocities near the phase velocity of the wave are resonant with the unstable ($\gamma_k > 0$) modes. In symmetric systems such as cases 1-3 and 5, the phase velocity $\mathbf{v}_k = (\omega_k/k)\hat{\mathbf{k}}$ is zero because the real frequency of the unstable modes is zero in the simulation frame (see Table I). Such particles can become trapped by the electrostatic potential and follow trapped orbits, generally with excursions in both $r_{||}$ and r_{\perp} . γ_k is symmetric under changes of sign of $k_{||}$ and k_{\perp} and as a result the resonant region of velocity for species j is enclosed by a diamond (except for the special case $k_{\perp} = 0$) given by

$\hat{\mathbf{k}} \cdot (\mathbf{v} - \mathbf{v}_k) = \pm v_{tr,j}$ where the trapping width $v_{tr,j}$ is given by $v_{tr,j}/v_{tj} = 2\sqrt{e|Z_j|\phi/T_j}$. For a system dominated by the fastest-growing linear mode, $\mathbf{k} = (\pm k_{||}^{max}, \pm k_{\perp}^{max})$. Z_j is the charge state of species j and ϕ is a potential that characterizes the half-depth of the potential well experienced by the particles.

In Fig. 3, regions in velocity space resonant with $\langle f_i \rangle$ are shown for the modes $\mathbf{k} = \mathbf{k}^{max}$ (see Table I). Regions bound by both $v_{tr,i}^{max} = v_{tr,i}(0.5[\max(\Phi) - \min(\Phi)])$, and $v_{tr,i}^{RMS} = v_{tr,i}[\text{RMS}(\Phi)]$ are indicated by dotted and dashed lines, respectively. RMS denotes a root-mean-squared value, calculated by averaging over the entire system. $v_{tr,i}^{max}$ defines the furthest extent of resonant interaction, while $v_{tr,i}^{RMS}$ is an approximate average over the 2D structures in Φ . The arrows indicate the direction of the trapped ion oscillations. Not shown, the electron distribution function f_e is also modified, exhibiting a trapping-induced flattening of a few percent centered about \mathbf{v}_k . While this modification of f_e does not appear to impact the evolution of the IISI, it may be of importance to other processes not investigated here.

By examining $v_{tr,i}$, it is apparent that the amplitude of a mode driven by the IISI is limited to the intersection of the resonant region with the bulk of the ion distribution in cases 1-3 (known as wave breaking³¹). i.e., Φ will grow until $v_{tr,i}^{RMS} \simeq \hat{\mathbf{k}}^{max} \cdot \mathbf{u}_i$, which is accurate to within 10% for cases 1-3. After saturation of the $\mathbf{k} \sim \mathbf{k}^{max}$ modes, the spectrum becomes sufficiently broad such that Φ causes a diffusion in velocity space, fully stabilizing the IISI.

In cases 1, 2, and 3, the average flow velocity defined as $u_i(t) = \langle \int_{\mathbf{v}} v_{||} f_i d\mathbf{v} \rangle / n_i$ approaches a reduction in magnitude by 30%, 38%, and just 4%, respectively, shown in Fig. 1b. However, the maximum of $\langle f_i \rangle$ in velocity space moves little if at all, as is apparent in Fig. 3. In fact, for case 2, the position of the maximum *increases* in magnitude by 14% relative to its initial value due to particles being pulled away by trapping predominantly from the side of f closest to the resonance. We define the time-varying spatially-averaged directional temperature as $\mathbf{T}_j = (m_j/n_j) \langle \int_{\mathbf{v}} (\mathbf{v} - \mathbf{u}_j)^2 f_j d\mathbf{v} \rangle$. This is the temperature that a Maxwellian distribution of species j would need in order to have a kinetic energy equal to that of f_j in the frame moving at \mathbf{u}_j , calculated independently for the parallel and perpendicular directions. \mathbf{T}_j is shown for cases 1-3 in Fig. 1c. Despite f_e exhibiting flattening near $v = 0$ due to trapping, T_e deviates from its initial value by only $\sim 1\%$.

For supersonic flows, the scalings of the final flow velocities and temperatures with the initial flow velocities follow from the behavior of \mathbf{k}^{max} : at higher flow velocities, the most unstable mode moves to larger angles relative to the flow (so that $\mathbf{k}^{max} \cdot \mathbf{u}$ approximately satisfies the acoustic dispersion relation), and the action of trapping on the distribution is likewise directed at larger angles relative to the flow. In case 3, the ion bounce motion is almost perpendicular to the flow, resulting in almost ex-

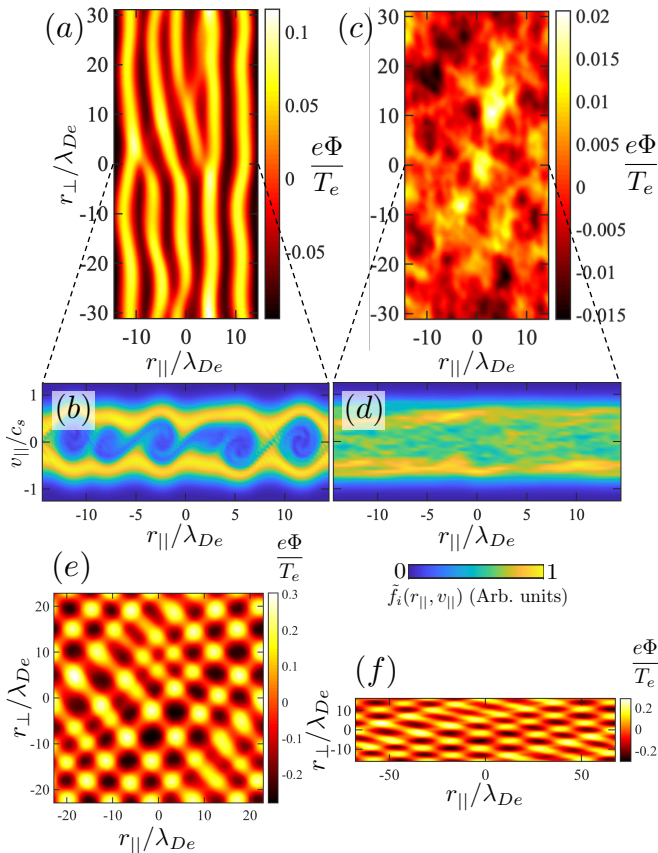


FIG. 4. For case 1, the (a,c) electrostatic potential and the (b,d) total ion distribution, sampled at $r_{\perp} = 0$ and integrated over v_{\perp} . Snapshots (a) and (b) are taken at the maximum in time of the total field energy, while (c) and (d) are the final state of the simulation. (e,f) The electrostatic potential in cases 2 and 3, respectively, taken at the maximum in time of the total field energy.

clusively transverse ion heating and little slowing down. However, the final value of $T_{i\parallel}$ is not simply a monotonic function of u/c_s . As u decreases to subsonic values and the IISI becomes effectively one-dimensional (as in case 1), one has at saturation $v_{tr,i}^{RMS} = uk_{\parallel}^{max}$ and the final value of $T_{i\parallel}$ falls accordingly until, for sufficiently low u , the instability is simply below threshold and does not occur.

A quasilinear description, such as that explored by Forslund⁵, is in qualitative agreement with the results shown for cases 1-3, correctly recovering that perpendicular ion heating dominates parallel heating at high flow velocities and that the slowing down due to the IISI for symmetric single-ion species flows is modest. However, any feature of a kinetic simulation that is a direct consequence of trapping will be missed by a quasilinear treatment. For example, a quasilinear model will not include the excursion of trapped ions to a distance $v_{tr,i}$ beyond the point in velocity space at which they are resonant, leading to a significant underestimate of the final perpendicular ion temperature for supersonic flows: in case 3, one has $T_{i\perp}/T_e \approx 0.5$, whereas the prediction from a quasilinear model⁵ is $T_{i\perp}/T_e \approx 0.25$.

B. Multi-ion species flows

We now consider case 4 (see Table I), where one stream is entirely comprised of hydrogen (H) ions and the other is fully-ionized carbon (C). The initial ion temperatures and number densities are equal. Shown in Fig. 5a and

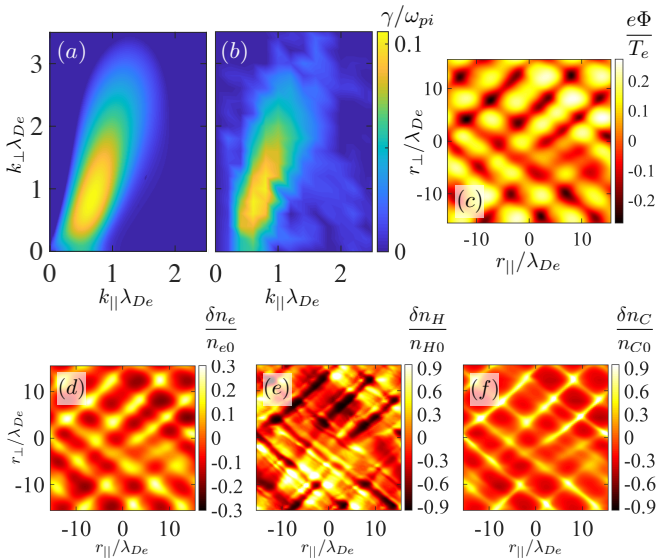


FIG. 5. For case 4, the (a) theoretical linear kinetic growth rate, and (b) measured growth rate γ of the ion streaming instability in a simulation. (c) Potential Φ and (d) electron, (e) hydrogen ion, and (f) carbon ion density modulations δn_j relative to initial values n_{j0} excited by the ion streaming instability.

5b, the theoretical linear kinetic growth rate and the measured numeric growth rate are again in quantitative agreement. In Fig. 5c, Φ taken at the maximum in time of E_{es} is shown. The structure of Φ is qualitatively similar to case 2 due to the similar range of unstable modes. However, in cases 1-3, the electron and ion density modulations are in phase. In contrast, the electrons and C ions are in phase in case 4, while the H ions [notably with $\mathcal{O}(1)$ density modulations] are approximately anti-phased. In fact, the phase relationship between each component (shown at the peak of E_{es} in Figs. 5d-f) evolves as T_j increases in time, similar to the “slow mode” described in Refs. 32 and 33.

The trapping widths of H and C ions are given by $v_{tr,i}/c_s = 2\sqrt{Z_i/A_i}\sqrt{e\phi/T_e}$ and therefore $v_{tr,H}/v_{tr,C} = \sqrt{2}$, where A_i is the ion mass number. As a result, the conventional wave-breaking limit³¹ of H ions (when the trapping width intersects the bulk) will be reached before that of the C ions. The evolution of $\langle f_i \rangle$ for case 4 is shown in Fig. 6, and the associated energy partitioning, flow velocity, and temperature evolution in time are

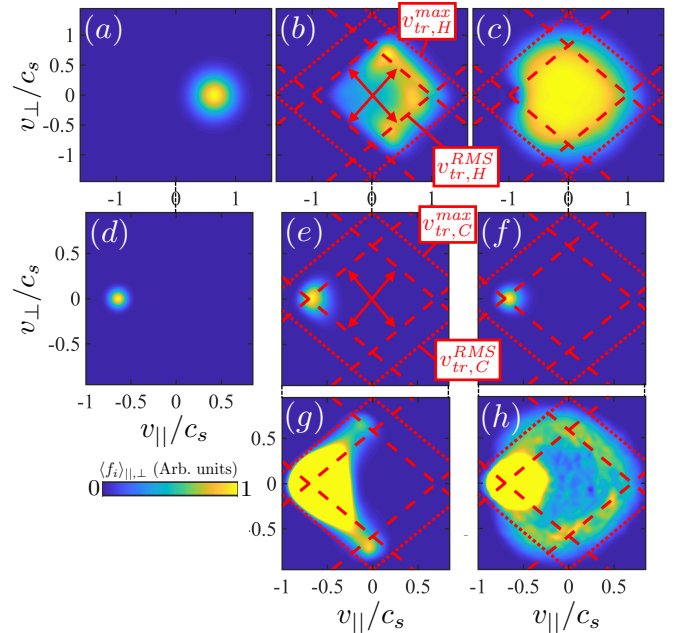


FIG. 6. Snapshots of the evolving spatially-averaged (a-c) hydrogen, f_H , and (d-f) carbon, f_C , distributions for case 4. Shown are the initial distributions (left column), the distributions when the field energy is at a maximum (middle column), and the final state of the distribution taken at the end of the simulation (right column). Red lines indicate the calculated region of ion trapping associated with the maximum (max) or root-mean-squared (RMS) amplitude of the most unstable Fourier-mode in each case, while arrows indicate the direction of bounce motion. Note that due to the differing ion masses, one has $v_{tr,H}/v_{tr,C} = \sqrt{2}$. In panels (g) and (h), the color scale of (e) and (f), respectively, has been saturated at 0.3% of the maximum value in order to show detail in the tails of the distribution.

shown in Fig. 7.

As before, the most unstable linear IISI mode and ion trapping together dictate the structure in velocity space. However, in this case the H ions alone are not able to saturate the growth of the IISI by trapping: $v_{tr,j}$ grows until the resonant region fully encompasses the entire H ion distribution (Fig. 6c), and is instead saturated by trapping of the C ions (at the C ion wave breaking limit) where $v_{tr,C}^{RMS} \simeq \hat{\mathbf{k}}^{max} \cdot \mathbf{u}_C$. Note that for the phase velocity of the most unstable mode one has $v_k = \omega_k^{max}/k^{max} \ll$

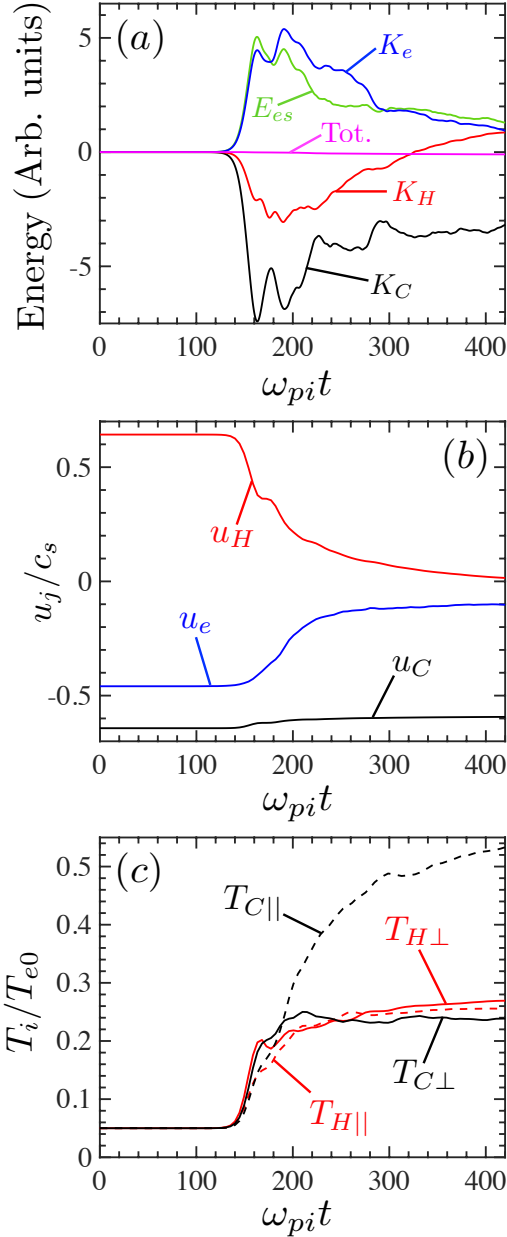


FIG. 7. For case 4, changes in the (a) per-species kinetic K_j , electrostatic E_{es} , and total (Tot.) energies, relative to initial values; (b) flow velocities u_j ; and (c) ion heating parallel (||) and perpendicular (\perp) to the flow direction.

$\hat{\mathbf{k}}^{max} \cdot \mathbf{u}_j$ (see Table I) and therefore the center of the resonance is far from the bulk of either ion distribution. This greater likelihood of H ions to become trapped due to their larger trapping width relative to C ions is then reinforced by the time required for ions to complete a trapped orbit: for the bounce frequency of a trapped particle one has $\omega_{b,j} = k\sqrt{e|Z_j|\phi/m_j}$ and the time taken to complete a trapped orbit is $\tau_{b,j} = 2\pi/\omega_{b,j}$. As ϕ falls during the latter stages of the evolution of the system, $\tau_{b,j}$ becomes large and ions may not fill out phase space as fully as if they were to experience an adiabatically decreasing amplitude. This effect is more pronounced for the C ions since $\tau_{b,C}/\tau_{b,H} = \sqrt{2}$. The longer bounce period of the C ions is readily apparent in the kinetic energy oscillations shown in Fig. 7a (compare K_H and K_C).

As a result of the total trapping of the H ions, the average flow speed of the H ions becomes that of the dominant IISI mode, which initially has $v_k \ll \hat{\mathbf{k}}^{max} \cdot \mathbf{u}_j$, i.e., the H ions are effectively stopped by the C ions due to the IISI. Conserving momentum, the C ions are also slowed, but to a lesser degree ($\sim 8\%$) due to their larger mass (see Fig. 7b). The electrons cancel out the current of the ions and so are slowed relative to their initial speed by an amount similar to the slowing of the ions, although this slowing is small ($\sim 1\%$) compared to v_{te} . As in the previous section, the electron distribution is flattened by a few percent but does not deviate from its initial temperature by more than $\sim 1\%$. In Fig. 7c, the evolution of \mathbf{T}_j is shown. The heating of the C ions in the direction parallel to the flow is striking ($T_{C||}/T_e \rightarrow \sim 0.5$) and exceeds the perpendicular C ion heating or the H ion heating in either direction by a factor of 2, while as before T_e is effectively unchanged. Analysis of $\langle f_C \rangle$ reveals a ring-like formation (Fig. 6f) that is qualitatively similar to case 2 (Fig. 3f).

Finally, we discuss case 5, where we simulate counterstreaming flows of CH_2 . Here, there are two symmetric counterstreaming flows of C ions and two symmetric counterstreaming flows of H ions, where there are twice as many H ions as C ions and initially one has $\mathbf{u}_{H,C} = (\pm u, 0)$. As before, growth rates for the IISI from theory and our simulations (not shown) agree in the linear stage, and this case is qualitatively similar to case 4. However, due to the symmetry of case 5, the flow of H ions is now separated from the flow of C ions in each stream: the H ions are trapped more readily than the C ions, and are pulled towards the center of the frame by the action of the IISI. This phenomenon of velocity separation is readily apparent in Fig. 8a, showing the C ions slowing by $\sim 26\%$ and H ions slowing by $\sim 50\%$. The C ion heating shown in Fig. 8b is even stronger than in case 4, most notably in the transverse direction, resulting in $T_{C\perp}/T_e \rightarrow \sim 1.5$ and $T_{C||}/T_e \rightarrow \sim 0.8$ ($T_{H||,\perp}/T_e \rightarrow \sim 0.25$, unchanged from case 4).

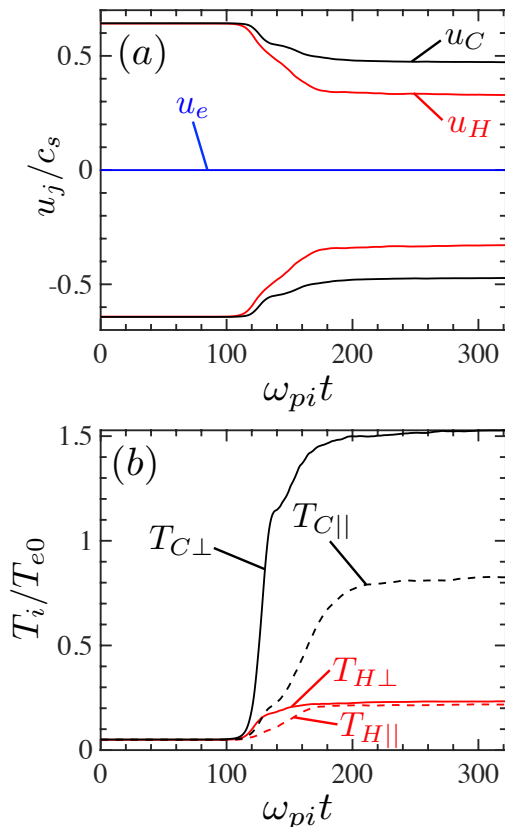


FIG. 8. For case 5, the per-species evolution of the (a) flow velocities u_j and (b) ion heating parallel (\parallel) and perpendicular (\perp) to the flow direction. This case highlights the velocity separation of the different ion species through the action of the IISI.

IV. CONCLUSIONS

We have studied the action of the ion-ion streaming instability (IISI) for single- and multi-ion species flows. The linear stage of evolution, and the subsequent initial saturation by trapping, is uncomplicated: in high-fidelity 2D2V Vlasov simulations, the most unstable modes are those predicted by linear theory, and the amplitude of the unstable modes is limited by ion trapping (the intersection of the trapping width with the bulk of the ion distribution, or “wave breaking”). The degree of ion heating parallel or perpendicular to the flow is dictated by the wave vector of the most unstable mode, with perpendicular heating dominating at higher flow velocities.

In plasma flows containing multiple ion species of differing charge-to-mass ratios, the trapping widths of each species will differ. Trapping of the lighter ion species alone may be insufficient to saturate the IISI; saturation instead occurs when the trapping width of the heavier ion species intersects the bulk of its distribution. The degree of heating and slowing of each species in the flow may be qualitatively different. This provides a mechanism for species (including isotope) separation in velocity and, in

a non-periodic system, space.

In collisionless shocks, the anisotropic heating of ions by the IISI has been observed in single-ion species simulations¹⁴ to give rise to a complicated picture, with simultaneous distinct Weibel instabilities arising from ions reflected at the shock front and from the temperature anisotropy driven by the IISI. Interpreting structures excited by Weibel instabilities may require careful consideration of the role of the IISI in modifying the plasma conditions from which other slower instabilities may grow, particularly if multiple ion species are present. In plasmas with some degree of collisionality, the IISI will also modify the collisional drag and heating by reducing relative flow speeds, as in cases 1-4, or indeed by introducing a relative flow as in case 5 (counterstreaming flows of CH₂), where the hydrogen ions are slowed more than the carbon ions within each flow.

ACKNOWLEDGMENTS

We are pleased to acknowledge valuable discussions with Wojciech Rozmus. This work was performed under the auspices of the U.S. Department of Energy by Lawrence Livermore National Laboratory under Contract DE-AC52-07NA27344 and funded by the Laboratory Research and Development Program at LLNL under project tracking code 17-ERD-081. Computing support for this work came from the Lawrence Livermore National Laboratory (LLNL) Institutional Computing Grand Challenge program. B. J. Winjum acknowledges support from DOE under Grant No. DE-SC0019010 and UCOP under Grant No. LFR-17-449059. This document was prepared as an account of work sponsored by an agency of the United States government. Neither the United States government nor Lawrence Livermore National Security, LLC, nor any of their employees makes any warranty, expressed or implied, or assumes any legal liability or responsibility for the accuracy, completeness, or usefulness of any information, apparatus, product, or process disclosed, or represents that its use would not infringe privately owned rights. Reference herein to any specific commercial product, process, or service by trade name, trademark, manufacturer, or otherwise does not necessarily constitute or imply its endorsement, recommendation, or favoring by the United States government or Lawrence Livermore National Security, LLC. The views and opinions of authors expressed herein do not necessarily state or reflect those of the United States government or Lawrence Livermore National Security, LLC, and shall not be used for advertising or product endorsement purposes.

¹J. S. Ross, S. H. Glenzer, P. Amendt, R. Berger, L. Divol, N. L. Kugland, O. L. Landen, C. Plechaty, B. Remington, D. Ryutov, W. Rozmus, D. H. Froula, G. Fiksel, C. Sorce, Y. Kuramitsu, T. Morita, Y. Sakawa, H. Takabe, R. P. Drake, M. Grosskopf, C. Kuranz, G. Gregori, J. Meinecke, C. D. Murphy, M. Koenig, A. Pelka, A. Ravasio, T. Vinci, E. Liang, R. Presura,

- A. Spitkovsky, F. Miniati, and H.-S. Park, *Phys. Plasmas* **19**, 056501 (2012), <https://doi.org/10.1063/1.3694124>.
- ²J. S. Ross, H.-S. Park, R. Berger, L. Divol, N. L. Kugland, W. Rozmus, D. Ryutov, and S. H. Glenzer, *Phys. Rev. Lett.* **110**, 145005 (2013).
- ³H.-S. Park, C. M. Huntington, F. Fiuza, R. P. Drake, D. H. Froula, G. Gregori, M. Koenig, N. L. Kugland, C. C. Kuran, D. Q. Lamb, M. C. Levy, C. K. Li, J. Meinecke, T. Morita, R. D. Petrasso, B. B. Pollock, B. A. Remington, H. G. Rinderknecht, M. Rosenberg, J. S. Ross, D. D. Ryutov, Y. Sakawa, A. Spitkovsky, H. Takabe, D. P. Turnbull, P. Tzeferacos, S. V. Weber, and A. B. Zylstra, *Phys. Plasmas* **22**, 056311 (2015), <https://aip.scitation.org/doi/pdf/10.1063/1.4920959>.
- ⁴T. E. Stringer, *J. Nucl. Energy, Part C* **6**, 267 (1964).
- ⁵D. W. Forslund and C. R. Shonk, *Phys. Rev. Lett.* **25**, 281 (1970).
- ⁶G. F. Krymskii, *Akademiia Nauk SSSR Doklady* **234**, 1306 (1977).
- ⁷W. I. Axford, E. Leer, and G. Skadron, *International Cosmic Ray Conference* **11**, 132 (1977).
- ⁸A. R. Bell, *MNRAS* **182**, 147 (1978), <http://oup.prod.sis.lan/mnras/article-pdf/182/2/147/3710138/mnras182-0147.pdf>.
- ⁹A. R. Bell, *MNRAS* **182**, 443 (1978), <http://oup.prod.sis.lan/mnras/article-pdf/182/3/443/3856040/mnras182-0443.pdf>.
- ¹⁰R. D. Blandford and J. P. Ostriker, *Astrophysical Journal, Part 2 - Letters to the Editor* **221**, L29 (1978).
- ¹¹D. Haberberger, S. Tochitsky, F. Fiuza, C. Gong, R. A. Fonseca, L. O. Silva, W. B. Mori, and C. Joshi, *Nat. Phys.* **8**, 95 (2012).
- ¹²O. Tresca, N. P. Dover, N. Cook, C. Maharjan, M. N. Polyanskiy, Z. Najmudin, P. Shkolnikov, and I. Pogorelsky, *Phys. Rev. Lett.* **115**, 094802 (2015).
- ¹³A. Pak, S. Kerr, N. Lemos, A. Link, P. Patel, F. Albert, L. Divol, B. B. Pollock, D. Haberberger, D. Froula, M. Gauthier, S. H. Glenzer, A. Longman, L. Manzoor, R. Fedosejevs, S. Tochitsky, C. Joshi, and F. Fiuza, *Phys. Rev. Accel. Beams* **21**, 103401 (2018).
- ¹⁴T. N. Kato and H. Takabe, *Phys. Plasmas* **17**, 032114 (2010), <https://doi.org/10.1063/1.3372138>.
- ¹⁵W. shuai Zhang, H. bo Cai, and S. ping Zhu, *Plasma Phys. Control. Fusion* **60**, 055001 (2018).
- ¹⁶R. Kumar, Y. Sakawa, L. N. K. Döhl, N. Woolsey, and A. Morace, *Phys. Rev. Accel. Beams* **22**, 043401 (2019).
- ¹⁷B. D. Fried and A. Y. Wong, *Phys. Fluids* **9**, 1084 (1966), <https://aip.scitation.org/doi/pdf/10.1063/1.1761806>.
- ¹⁸D. Grésillon, F. Doveil, and J. M. Buzzi, *Phys. Rev. Lett.* **34**, 197 (1975).
- ¹⁹E. A. Foote and R. M. Kulsrud, *The Physics of Fluids* **24**, 1532 (1981), <https://aip.scitation.org/doi/pdf/10.1063/1.863568>.
- ²⁰H. Karimabadi, N. Omid, and K. B. Quest, *Geophys. Res. Lett.* **18**, 1813 (1991).
- ²¹J. Banks and J. Hittinger, *IEEE Trans. Plasma Sci.* **38**, 2198 (2010).
- ²²J. W. Banks, R. L. Berger, S. Brunner, B. I. Cohen, and J. A. F. Hittinger, *Phys. Plasmas* **18**, 052102 (2011).
- ²³J. W. Banks, A. G. Odu, R. L. Berger, T. Chapman, W. T. Arrighi, and S. Brunner, Accepted for publication in *SIAM J. Sci. Comput.* and awaiting publication online (<https://doi.org/10.1137/19M1238551>) (2019).
- ²⁴A. Kumar and V. Mathew, *Physics of Plasmas* **24**, 092107 (2017), <https://doi.org/10.1063/1.4989427>.
- ²⁵W. Oohara and R. Hatakeyama, *Phys. Rev. Lett.* **91**, 205005 (2003).
- ²⁶J. Vranjes and S. Poedts, *Plasma Sources Science and Technology* **14**, 485 (2005).
- ²⁷R. L. Berger, J. R. Albritton, C. J. Randall, E. A. Williams, W. L. Kruer, A. B. Langdon, and C. J. Hanna, *Phys. Fluids B* **3**, 3 (1991), <https://doi.org/10.1063/1.859954>.
- ²⁸R. A. Fonseca, L. O. Silva, F. S. Tsung, V. K. Decyk, W. Lu, C. Ren, W. B. Mori, S. Deng, S. Lee, T. Katsouleas, and J. C. Adam, *Lecture Notes in Computer Science* **2331**, 342 (2002).
- ²⁹T. Chapman, R. L. Berger, B. I. Cohen, J. W. Banks, and S. Brunner, *Phys. Rev. Lett.* **119**, 055002 (2017).
- ³⁰B. D. Fried and S. D. Conte, *The Plasma Dispersion Function* (Academic Press, New York, 1961).
- ³¹W. L. Kruer, *The Physics of Laser Plasma Interactions* (Westview Press, Boulder, CO, 2003).
- ³²E. A. Williams, R. L. Berger, R. P. Drake, A. M. Rubenchik, B. S. Bauer, D. D. Meyerhofer, A. C. Gaeris, and T. W. Johnston, *Phys. Plasmas* **2**, 129 (1995), <https://doi.org/10.1063/1.871101>.
- ³³T. Chapman, R. L. Berger, S. Brunner, and E. A. Williams, *Phys. Rev. Lett.* **110**, 195004 (2013).